The Journal of Fluid Control
including FLUIDICS QUARTERLY

FLUID CONTROL, HYDRAULICS & PNEUMATICS, INSTRUMENTATION AND FLUIDICS

J. Y. Lai, C. H. Menq and R. Singh, Fluid Power Laboratory, Department of Mechanical Engineering The Ohio State University, Columbus OH

Methods to analyze the characteristics of a valve-controlled pneumatic chamber under the PWM mode in both frequency and time domains are presented, and a PI control strategy for this system is proposed. A dual Fourier expansion method is used to obtain the transfer characteristics of the PWM and a first-order chamber model having flow direction dependent system parameters is employed to study the chamber frequency response. The steady-state behavior of the governing differential equations is obtained through time domain solutions. Predicted results of the frequency response are found to agree extremely well with the measurements obtained. Simulation results also reveal that the carrier frequency significantly affects the steady-state pressure response. Moreover, the feasibility of using a PI controller is demonstrated successfully through an experiment. The effect of the proportional and integral gains are also discussed.

VOLUME NINETEEN, NUMBER FOUR

PUBLICATION DATE JANUARY 1989

DELBRIDGE PUBLISHING COMPANY

A MESSAGE FROM THE EDITOR

For this issue

J. Y. Lai, C. H. Menq and R. Singh from The Ohio State University present their study of methods for the analysis of the operational characteristics of a valve-controlled pneumatic chamber in the PWM mode (both frequency and time). They have also developed a PI control for this system. Their analysis conforms well to the results of their experimental studies. (Fluid Power Laboratory, Department of Mechanical Engineering, The Ohio State University, 206 West 18th Avenue, Columbus OH 43210.)

PRESSURE CONTROL OF A PNEUMATIC CHAMBER

J.Y. Lai, C.H. Menq and R. Singh, Fluid Power Laboratory, Department of Mechanical Engineering
The Ohio State University, Columbus OH

Pulse-width-modulation (PWM) has been found to be very effective in the control of dc motors and hydraulic servos because the technique reduces the effect of such nonlinearities as hysteresis, threshold and stiction, and improves system reliability and performance. It has also been applied to on-off controlled pneumatic actuators to modulate the valve performance by Noritsugu [References 8 and 9] and Morita et al. [Reference 7]. Noritsugu [Reference 9] employed two valves under on-off control, and a third valve (automotive injection valve) under the PWM control when operating in the vicinity of the desired position. However, this scheme is too complex and costly. Morita et al. [Reference 7] and Noritsugu [Reference 8] have also implemented the PWM mode in pneumatic manipulators to

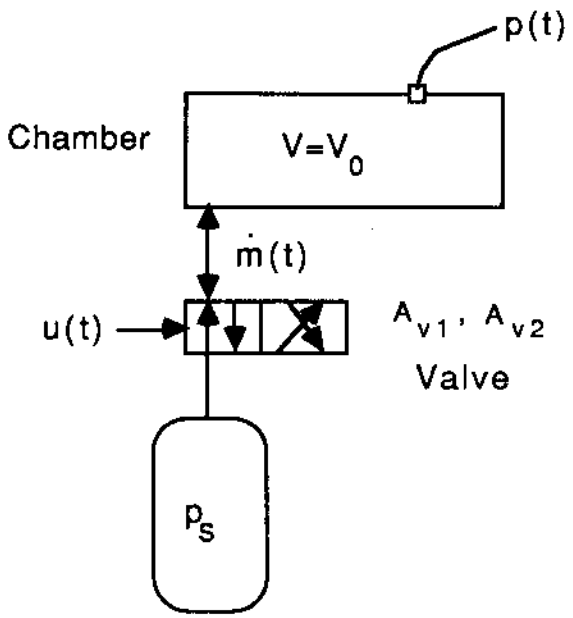

Figure 1a. Proposed System Schematic—Valve-Chamber System

control pressure and contact force, respectively. However, their models of mass flow characteristics fail to describe the on-off effect of valve motion. Moreover, the literature does not contain any analytical study on the effect of the PWM mode on the pneumatic system performance. This paper is intended to fill this void while proposing a better system model and a control strategy with a successful experimental demonstration.

Various attempts at modeling pneumatic actuators have been made. Shearer [Reference 11], Burrows [Reference 4], and Botting et al. [Reference 3] have used the transfer function approach to model the dynamics of pneumatic actuator systems. However, such a linearized model is suitable only for the mid-stroke position. Recently, Liu [Reference 6] and Scavanda [Reference 10] have used the state-space approach to extend the linear model to various operating positions. But, their approach ignores the effect of the discharge coefficient, which varies with the pressure ratio between the downstream and upstream sides of the valve, and the orifice geometry.

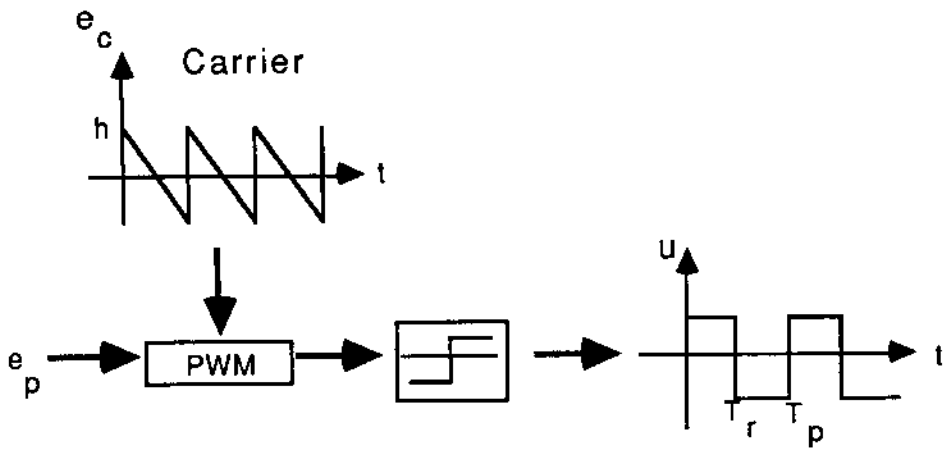

Figure 1b. Proposed System Schematic–Formulation of the PWM Mode

A number of techniques for force control of pneumatic manipulators have been proposed. Suh et al. [Reference 12] has carried out experimental work on an on-off controlled robot gripper to examine the effect of the various parameters on system performance. Morita's work [Reference 7], because it employed the PWM mode on the on-off valve, has demonstrated the feasibility of using PWM control. However, with only proportional feedback implemented, he and his co-workers found that there is a deviation between the command pressure and the mean pressure response. Noritsugu, as reported in Reference 8, successfully employed an analog PI control scheme to reduce the steady-state error.

In this paper, a pneumatic valve-controlled chamber system—shown schematically in Figure 1a—is studied. The on-off valve with a supply pressure p_s is operated under the PWM mode to control the chamber pressure $p(t)$. The chamber volume V is fixed, and the valve orifice area is A_{v1} for charging and A_{v2} for discharging. A periodic pulse signal $u(t)$ with a duty pulse width of T_r, which is proportional to the pressure error e_p [pressure difference between the actual $p(t)$ and the command chamber pressure $p_c(t)$], is input to the solenoid of the valve, as shown in Figure 1b. We extend the literature here by developing a flow direction dependent model in which the total pressure term, instead of the perturbed one, is used, and by including a realistic description of the discharge coefficients c_{d1} and c_{d2}. Based on this model, an analytical study of the effect of the PWM mode on the system performance is carried out in both frequency and time domains. Subsequently, a strategy is proposed to control the chamber pressure $p(t)$.

FREQUENCY RESPONSE

Chamber Dynamics

Assume that the ideal equation of state is valid, the thermofluid process is isentropic and the valve dynamics are neglected. Accordingly for the chamber we get

$$p(t)V = m(t)RT(t) \tag{1}$$

$$p(t)T^{\frac{n}{1-n}} = p_0 T_0^{\frac{n}{1-n}}$$

$$p_0 = p(0)$$

$$T_0 = T(0) \tag{2}$$

where m is mass, R is gas constant, T is temperature, t is time, and n is the isentropic constant, which is 1.4 for air. If the temperature $T(t)$ variations are very small, then $T(t) \approx T_0$, and using Equations 1 and 2, we get

$$\dot{p} = k_r \dot{m}$$

$$k_r = \frac{nRT_0}{V} \tag{3}$$

The mass flow rate $\dot{m}$ can be expressed as follows [Andersen, Reference 1]:

$$m = \begin{cases} \dfrac{C_{d1} A_{v1} P_s k N_{12}}{\sqrt{T}} & \text{for } u(t) > 0 \\ \dfrac{-C_{d2} A_{v2} P_4 k C_{24}}{\sqrt{T_0}} & \text{for } u(t) < 0 \end{cases} \tag{4}$$

where

$$C_{d1} = C_{a1} - C_{b1}\frac{p(t)}{p_s}$$

$$C_{d2} = C_{a2} + C_{b2}\frac{p(t)}{p_4}$$

$$k = \left[\frac{ng}{R}\left(\frac{2}{n+1}\right)^{\frac{n+1}{n-1}}\right]^{\frac{1}{2}}$$

$$N_{12} = \begin{cases} k_n \left[\left\{\dfrac{p(t)}{p_s}\right\}^{\frac{2}{n}} - \left\{\dfrac{p(t)}{p_s}\right\}^{\frac{n+1}{n}}\right]^{\frac{1}{2}} & \text{for } \dfrac{p(t)}{p_s} > r_c \\ 1 & \text{for } \dfrac{p(t)}{p_s} < r_c \end{cases}$$

(r_c = 0.528 for air)

$$C_{24} = k_n \left\{\frac{p_4}{p(t)}\right\}\left[\left\{\frac{p_4}{p(t)}\right\}^{\frac{2}{n}} - \left\{\frac{p_4}{p(t)}\right\}^{\frac{n+1}{n}}\right]^{\frac{1}{2}}$$

where p_4 is the atmospheric pressure, k_n is a constant (0.258 for air) and g is the gravitational constant. When $u(t) > 0$, air flows through the supply port of the valve to the chamber, and when $u(t) < 0$, air from the chamber escapes to the atmosphere. The discharge coefficients C_{d1} and C_{d2} are defined with respect to the input and output ports of the valve, respectively. Here

$$\begin{aligned} C_{a1} &= 0.53 \\ C_{b1} &= 0.01 \\ C_{a2} &= 0.231 \\ C_{b2} &= 0.121 \end{aligned}$$

In order to study the system characteristics, Equation 4 is linearized as

$$\dot{m} = -k_1 p + k_2 A_v \tag{5}$$

where

$$\begin{aligned} A_v &= A_{v1} \qquad \text{for } u(t) > 0 \\ A_v &= -A_{v2} \qquad \text{for } u(t) < 0 \\ k_1 &= \begin{cases} A_{v1}\left[\frac{C_{b1}}{p_s}\left(\bar{N}_{12} + n_{12p}\bar{p}\right) - C_{a1}n_{12p}\right] & \text{for } u(t) > 0 \\ A_{v2}\left[\frac{C_{b2}}{p_s}\left(\bar{C}_{24} + c_{24p}\bar{p}\right) - C_{a2}c_{24p}\right] & \text{for } u(t) < 0 \end{cases} \\ k_2 &= \begin{cases} C_{b1}n_{12p}\frac{\bar{p}^2}{p_s} + C_{a1}\left(\bar{N}_{12} - n_{12p}\bar{p}\right) & \text{for } u(t) > 0 \\ C_{b2}c_{24p}\frac{\bar{p}^2}{p_s} + C_{a2}\left(c_{24p}\bar{p} - \bar{C}_{24}\right) & \text{for } u(t) < 0 \end{cases} \end{aligned}$$

where $\bar{N}_{12}$ and $\bar{C}_{24}$ denote the operating values, and n_{12p} and c_{24p} represent the perturbation of N_{12} and C_{24} around the operating pressure $\bar{p}$, respectively. Here $\bar{p}$ is defined as the average pressure for each cycle of valve motion in the steady state. Note that due to the on-off effect of valve motion, k_1/k_2 depends upon the sign of $u(t)$. Substituting Equation 5 into Equation 3, we obtain the governing equation of the chamber pressure response around the equilibrium position.

$$\begin{aligned} \dot{p} + \tau p &= k_a A_v \\ \tau &= k_1 k_r \\ k_a &= k_2 k_r \end{aligned} \tag{6}$$

Equation 6 represents a first-order system model with a distinct gain k_a and time constant τ depending on the flow direction.

Transfer Characteristics of PWM

The method of obtaining the transfer characteristics is based on a dual Fourier series expansion in two variables [Black, Reference 2]. Consider that the input signal $e_p(t)$ to the pulse width modulator is a sinusoidal wave $E_0 \sin \omega t$, where E_0 is the amplitude and ω is the modulation frequency. The modulated signal $u(\omega t, \omega_c t)$ of the carrier frequency ω_c can be expressed as follows:

$$\begin{aligned} u(\omega_c t, \omega t) = \frac{1}{2} A_{00} &+ \sum_{n=1}^{\infty} [A_{n0} \cos n\omega t + B_{n0} \sin n\omega t] \\ &+ \sum_{m=1}^{\infty} [A_{0m} \cos m\omega_c t + B_{0m} \sin m\omega_c t] \\ &+ \sum_{m=1}^{\infty} \sum_{n=\pm 1}^{\pm\infty} [A_{nm} \cos(m\omega_c t + n\omega t) + B_{nm} \sin(m\omega_c t + n\omega t)] \end{aligned} \tag{7}$$

where

$$A_{nm} = \frac{1}{2\pi^2} \int_0^{2\pi} \int_0^{2\pi} u(\omega_c t, \omega t) \cos(m\omega_c t + n\omega t) d(\omega_c t) d(\omega t) \tag{8a}$$

$$B_{nm} = \frac{1}{2\pi^2} \int_0^{2\pi} \int_0^{2\pi} u(\omega_c t, \omega t) \sin(m\omega_c t + n\omega t) d(\omega_c t) d(\omega t) \tag{8b}$$

The first term in Equation 7 is the dc component of the pulses. The frequency components of the second term correspond to the frequency components of the modulating wave ω and its harmonics. The third term separates frequencies into the fundamental frequency ω_c of the pulses and its harmonics. The frequency components of the last term are given by the ensemble of all positive pairs formed by taking the sum and difference of integral multiples of each fundamental.

Note that the modulated signal $u(\omega_c t, \omega t)$ is a periodic square wave with constant period T_p and amplitude A_{v1} when the valve is open, and A_{v2} when the valve is closed, thus, $u(\omega_c t, \omega t)$ is given by

$$u(\omega_c t, \omega t) = \begin{cases} A_{v1} & \text{for } 0 \leq \omega_c t < (\pi + \frac{\pi}{h} E_0 \sin \omega t) \\ -A_{v2} & \text{for } (\pi + \frac{\pi}{h} E_0 \sin \omega t) \leq \omega_c t < 2\pi \end{cases} \tag{9}$$

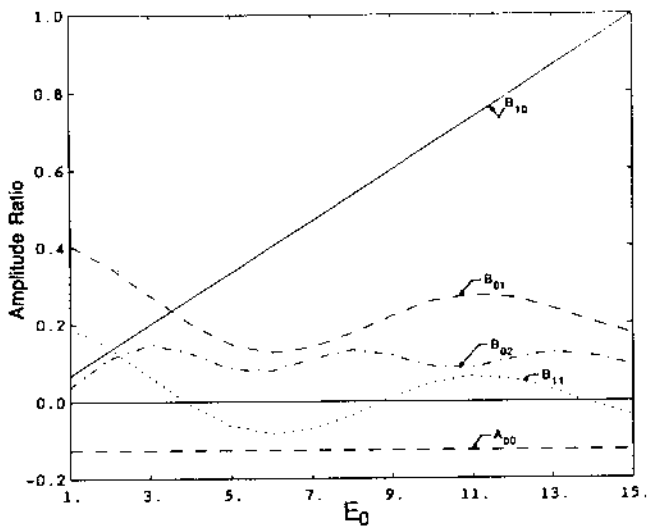

Figure 2. Effect of Input Amplitude E_0 on the Fourier Coefficients for the Modulated Signal (h = 0.00345 MPa, A_{v1} = 2.0E-4 m^2, A_{v2} = 4.45E-4 m^2)

where h is the amplitude of the carrier signal, as shown in Figure 1b. By substituting Equation 9 into Equation 8, A_{nm} and B_{nm} can be evaluated. The first few terms of the coefficients are given below

$$
\begin{aligned}
B_{10} &= \frac{E_0}{2h}(A_{v1} + A_{v2}) \\
B_{n0} &= 0 \qquad n = 2, 3, \ldots \\
B_{01} &= \frac{A_{v1} + A_{v2}}{2\pi^2} \left\{ \int_0^{2\pi} 1 + cos\left(\frac{\pi}{h} E_0 \, sin\, \omega t\right) \, d\omega t \right\} \\
B_{02} &= \frac{A_{v1} + A_{v2}}{4\pi^2} \left\{ \int_0^{2\pi} 1 - cos\left(\frac{2\pi}{h} E_0 \, sin\, \omega t\right) \, d\omega t \right\} \\
B_{11} &= \frac{A_{v1} + A_{v2}}{2\pi^2} \left\{ \int_0^{2\pi} cos\left[\left(\frac{\pi}{h} E_0 \, sin\, \omega t\right) + \omega t\right] \, d\omega t \right\}
\end{aligned}
\tag{10}
$$

Figure 2 shows the effect of the higher modes B_{01}, B_{02}, ..., etc., which induce small amplitude fluctuations in time domain response, cannot be neglected. Also, as E_0 is increased, B_{10} increases more significantly than B_{0m} and B_{1m}, and hence the effect of the carrier signal is reduced. Substituting the coefficients into Equation 7, we obtain

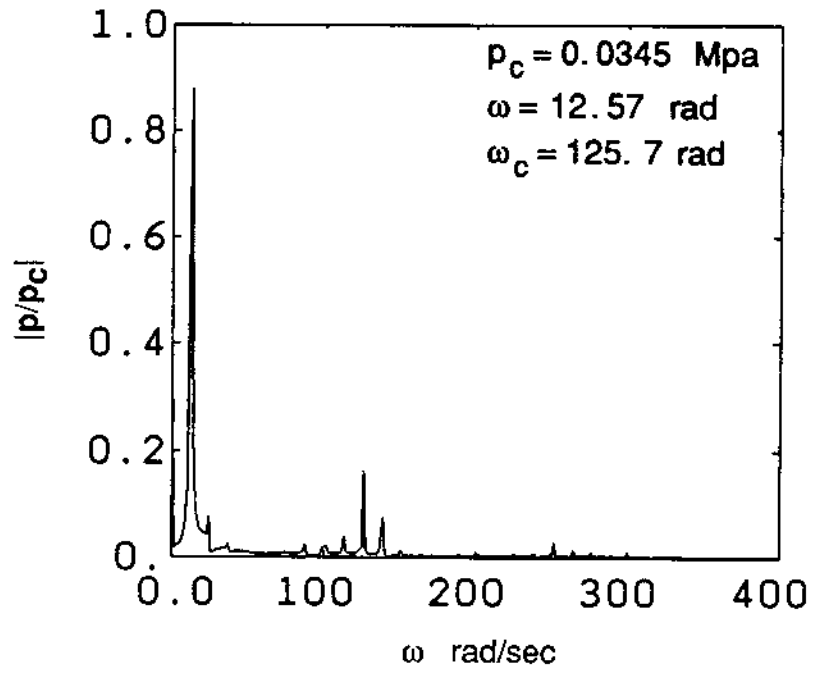

Figure 3a. Simulation of Output Frequency Spectra
(p_c = 0.0345 MPa, ω = 12.57 rad, ω_c = 125.7 rad)

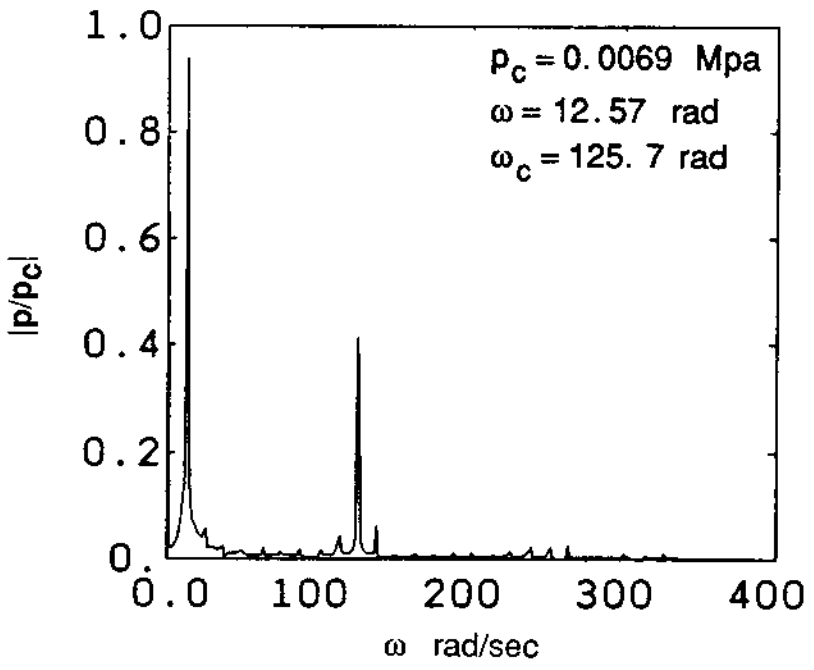

Figure 3b. Simulation of Output Frequency Spectra
(p_c = 0.0069 MPa, ω = 12.57 rad, ω_c = 125.7 rad)

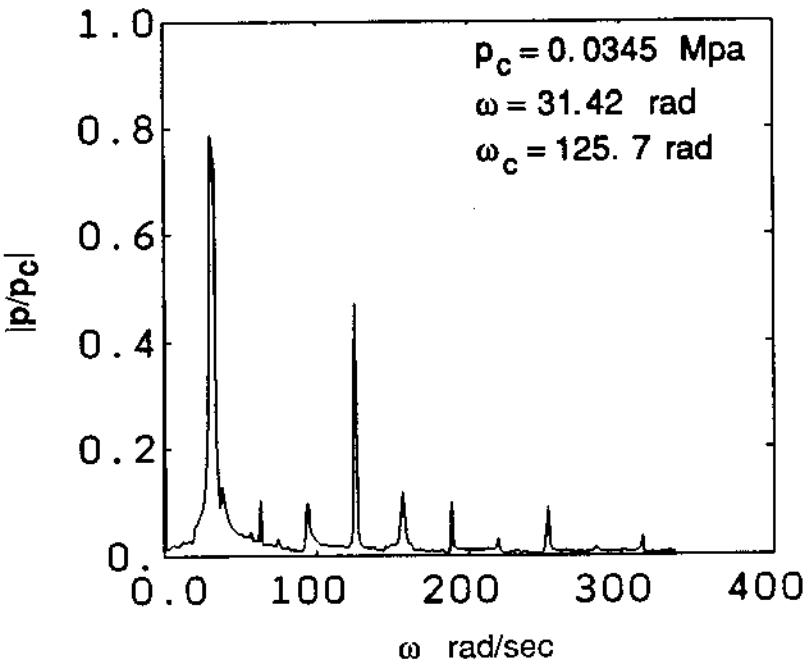

Figure 3c. Simulation of Output Frequency Spectra
(p_c = 0.0345 MPa, ω = 31.42 rad, ω_c = 125.7 rad)

$$u(\omega_c t, \omega t) = \frac{1}{2}A_{00} + B_{10}\, sin\, \omega t + \sum_{m=1}^{\infty} B_{0m}\, sin\, m\omega_c t + \sum_{m=1}^{\infty} B_{1m}\, sin(m\omega_c t \pm \omega t) \tag{11}$$

This shows that the modulated signal u is the superposition of the input signal, the carrier signal and the correlated terms between them. If the carrier frequency ω_c is larger than system bandwidth, the system can act as a low-pass filter to attenuate the high frequency component of the modulated signal. As the modulating frequency ω is increased, the effect of B_{1m} becomes more significant, which shows that the effect of the modulator increases.

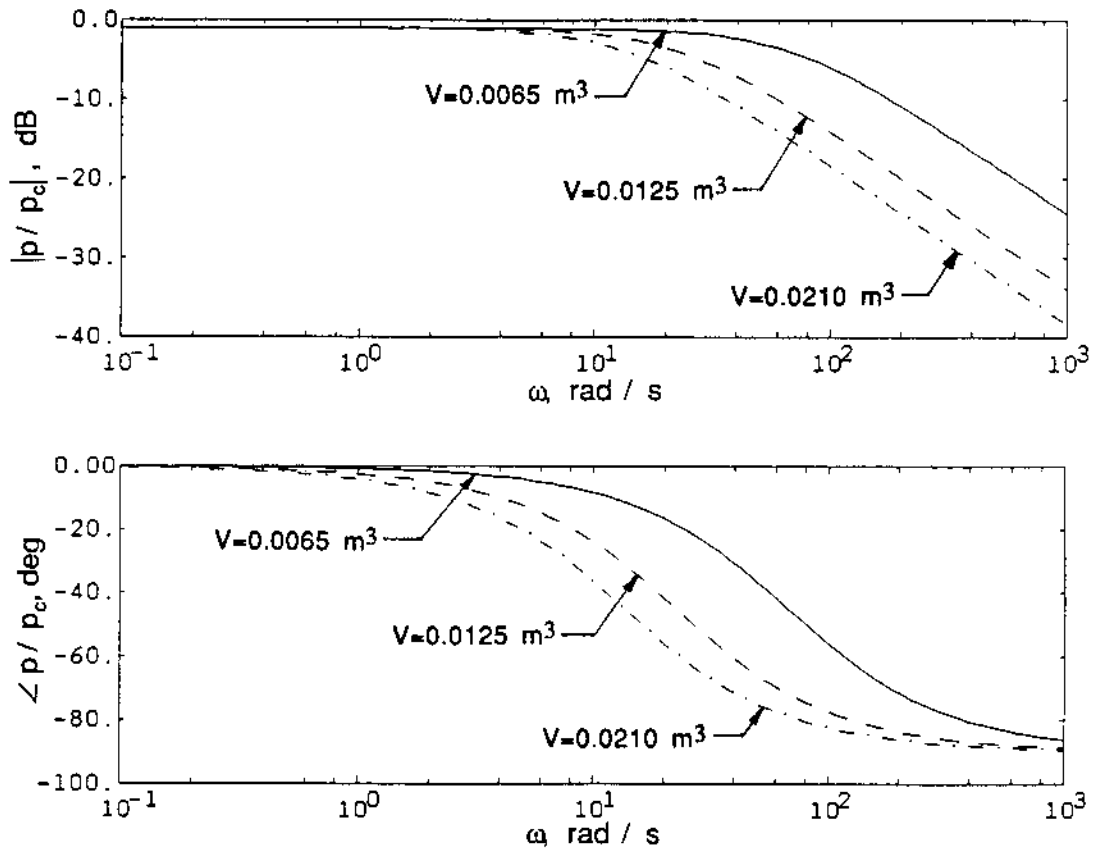

Figure 4. Effect of Volume V on System Frequency Response

Computer Simulation Results

To obtain the output frequency spectrum numerically, pressure $p(t)$ is fed back to form a closed-loop system, and the corresponding nonlinear model given by Equations 3 and 4 is used to represent the open-loop system. The command input p_c is a sinusoid. Figure 3 compares the normalized magnitude of the output frequency spectra for a number of cases. Figure 3a shows that the output spectrum contains the input frequency ω, the carrier frequency of 20 Hz and its higher harmonics, which are small. Figure 3b illustrates that as the input amplitude p_c is reduced, the effect of the carrier signal is increased. Figure 3c shows that as the input frequency ω is increased, the effect of the side frequencies becomes more significant, and hence the effect of the modulator is increased.

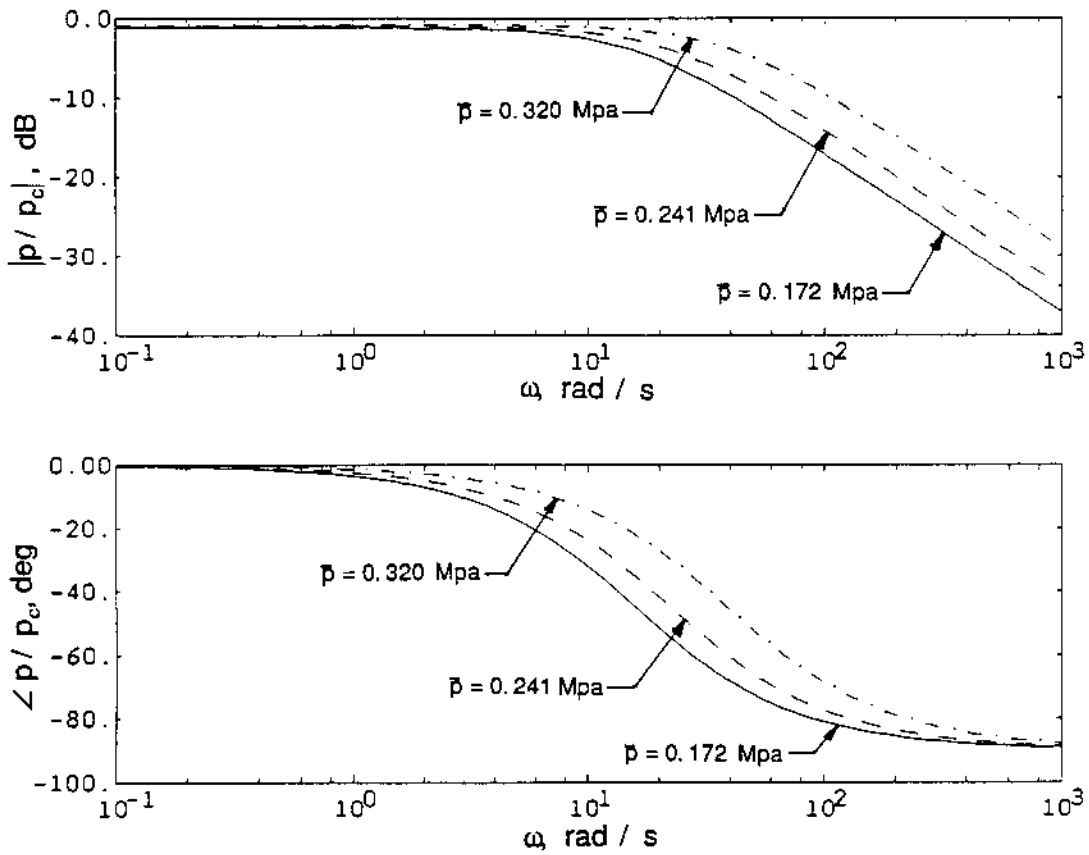

Figure 5. Effect of Operating Pressure $\bar{p}$ on System Frequency Response

The chamber model given by Equation 6 is used to study the closed-loop frequency response for a simplified $u(t)$ expressed as $E_0 \sin \omega t$. Figure 4 indicates that as the volume V is increased, the system bandwidth is reduced. Figure 5 shows that as the operating pressure $\bar{p}$ is increased, both the system bandwidth and the closed-loop gain are increased as well. For both cases it is expected that the steady-state error will appear because the system is a Type 0 system. Therefore, the use of the proportional control alone is not sufficient.

TIME DOMAIN RESPONSE p(t)

Since the frequency domain analysis does not provide sufficient information for the system performance, Equation 6 is solved to get the time domain behavior. Here $p(0)$ represents the initial pressure for the period con-

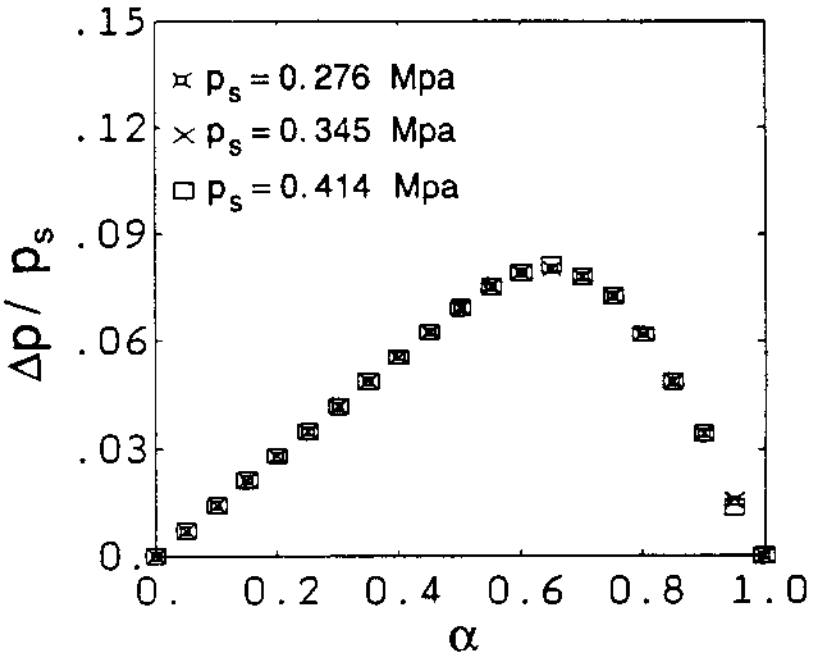

Figure 6a. Parametric Studies for Pressure Ripple Δp
Effect of Supply Pressure p_s

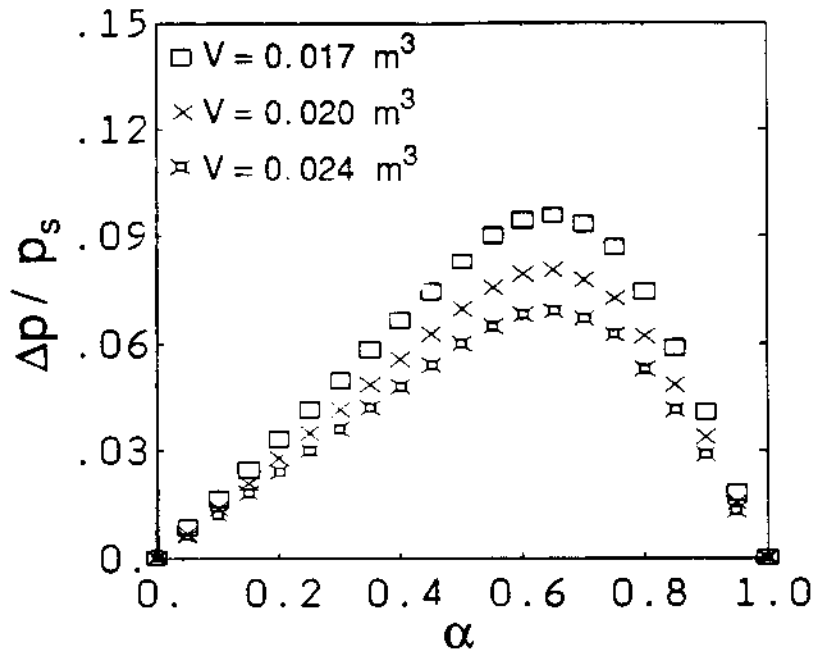

Figure 6b. Parametric Studies for Pressure Ripple Δp
Effect of Volume V

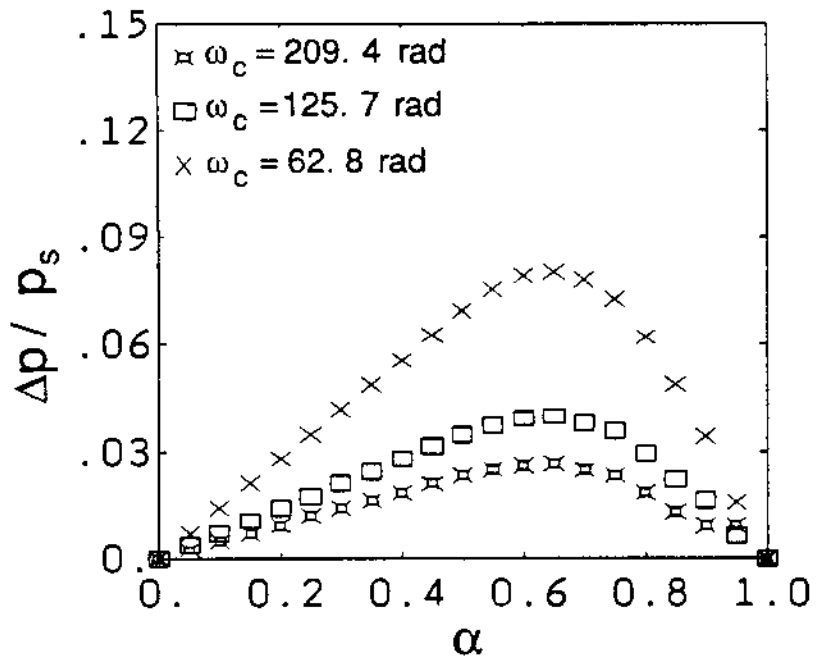

Figure 6c. Parametric Studies for Pressure Ripple Δp Effect of Carrier Frequency ω_c

sidered, $p(\alpha T)$ is the transient pressure when the pulse changes sign, and α is the duty factor. Accordingly, Equation 6 can be rewritten as

$$\frac{dp}{dt} + \tau_1 p = k_{a1} A_{v1} \qquad 0 \le t < \alpha T \tag{12a}$$

$$\frac{dp}{dt'} + \tau_2 p = -k_{a2} A_{v2} \qquad \alpha T \le t' < (1-\alpha)T \tag{12b}$$

where

$$\tau_1 = k_r A_{v1} \left[\frac{C_{b1}}{p_s} (\bar{N}_{12} + n_{12p}\bar{p}) - C_{a1} n_{12p} \right]$$

$$\tau_2 = k_r A_{v2} \left[\frac{C_{b2}}{p_s} (\bar{C}_{24} + c_{24p}\bar{p}) - C_{a2} c_{24p} \right]$$

$$k_{a1} = k_r \left[\frac{C_{b1} n_{12p} \bar{p}^2}{p_{s1}} + C_{a1} (\bar{N}_{12} - n_{12p}\bar{p}) \right]$$

$$k_{a2} = k_r \left[\frac{C_{b2} c_{24p} \bar{p}^2}{p_{s1}} + C_{a2} (c_{24p}\bar{p} - \bar{C}_{24}) \right]$$

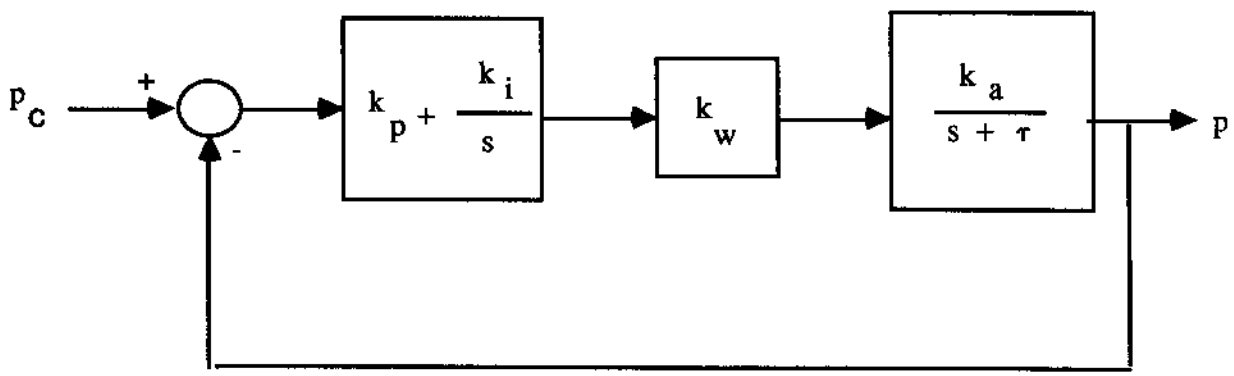

Figure 7. PI Control Block Diagram

Solving Equations 12a and l2b, we obtain

$$p(t) = \frac{k_{a1}A_{v1}}{\tau_1} + \left[p(0) - \frac{k_{a1}A_{v1}}{\tau_1}\right] e^{-\tau_1 t} \qquad 0 \le t < \alpha T \qquad (13a)$$

$$p(t') = -\frac{k_{a2}A_{v2}}{\tau_2} + \left[p(\alpha T) + \frac{k_{a2}A_{v2}}{\tau_2}\right] e^{-\tau_2 t} \quad 0 \le t' < (1-\alpha)T \qquad (13b)$$

Since the system is in the steady state, the following conditions can be observed:

$$p(t)|_{t=0} = p(t')|_{t'=(1-\alpha)T}$$
$$p(t)|_{t=\alpha T} = p(t')|_{t'=0}$$

Substitute these conditions into Equations 13a and 13b to obtain

$$p(0) = \frac{\frac{k_{a2}A_{v2}}{\tau_2}\left(e^{-\tau_2(1-\alpha)T} - 1\right) + \frac{k_{a1}A_{v1}}{\tau_1}e^{-\tau_2(1-\alpha)T}\left(1 - e^{-\tau_1\alpha T}\right)}{\left(1 - e^{-\tau_1\alpha T}e^{-\tau_2(1-\alpha)T}\right)} \qquad (14a)$$

$$p(\alpha T) = \frac{\frac{k_{a2}A_{v2}}{\tau_2}e^{-\tau_1\alpha T}\left(e^{-\tau_2(1-\alpha)T} - 1\right) + \frac{k_{a1}A_{v1}}{\tau_1}\left(1 - e^{-\tau_1\alpha T}\right)}{\left(1 - e^{-\tau_1\alpha T}e^{-\tau_2(1-\alpha)T}\right)} \qquad (14b)$$

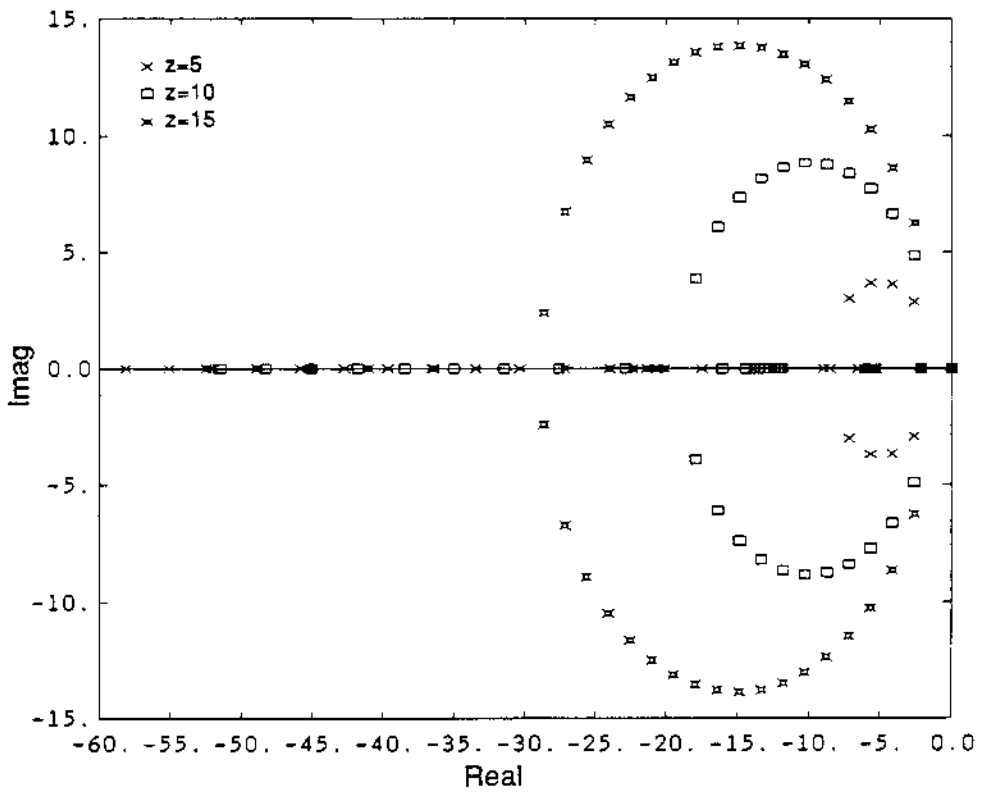

Figure 8. Root Locus Plot for the Closed-Loop System

Here, $p(0)$ and $p(\alpha T)$ are the minimum and maximum pressures, respectively, in the steady state. Accordingly, the pressure ripple Δp can then be expressed as

$$\begin{aligned}\Delta p &= p(\alpha T) - p(0) \\ &= \frac{\left(\frac{k_{a1}A_{v1}}{\tau_1} + \frac{k_{a2}A_{v2}}{\tau_2}\right)\left(e^{-\tau_2(1-\alpha)T} - 1\right)\left(e^{-\tau_1\alpha T} - 1\right)}{\left(1 - e^{-\tau_1\alpha T}e^{-\tau_2(1-\alpha)T}\right)}\end{aligned} \tag{15}$$

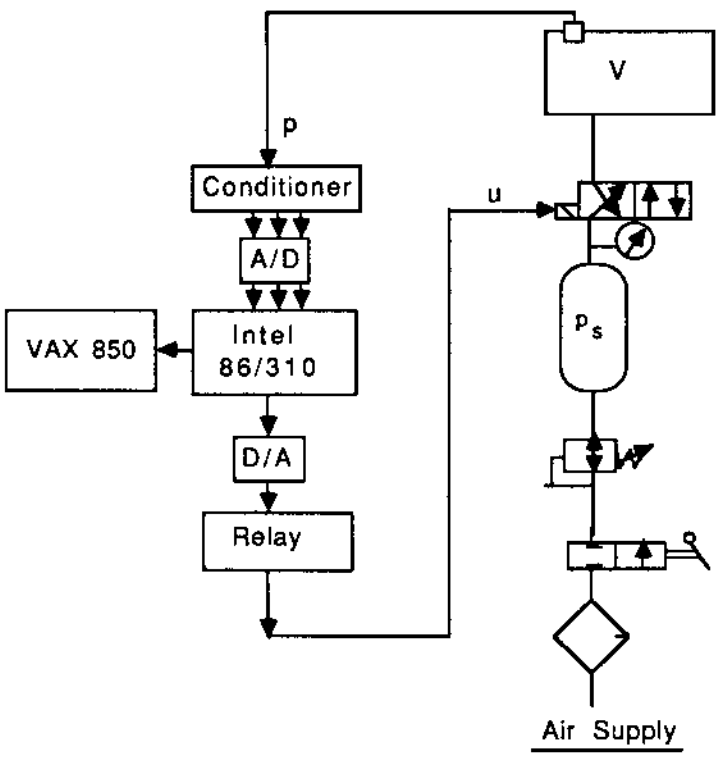

Figure 9. Experimental Schematic

and the average pressure $\bar{p}_a$ can be approximated as shown below by assuming that the steady-state profiles given by Equations 13a and 13b are linear.

$$\bar{p}_a = \frac{p(\alpha T) + p(0)}{2} \tag{16}$$
$$= \frac{\frac{k_{a2}A_{v2}}{\tau_2}\left(e^{-\tau_2(1-\alpha)T} - 1\right)\left(e^{-\tau_1\alpha T} + 1\right) + \frac{k_{a1}A_{v1}}{\tau_1}\left(e^{-\tau_2(1-\alpha)T} + 1\right)\left(1 - e^{-\tau_1\alpha T}\right)}{2\left(1 - e^{-\tau_1\alpha T}e^{-\tau_2(1-\alpha)T}\right)}$$

Figure 6 illustrates the effect of supply pressure p_s, volume V and carrier frequency ω_c on Δp, respectively. It should be noted that when the system is operated in the PWM mode, the pressure ripples Δp always exist. We

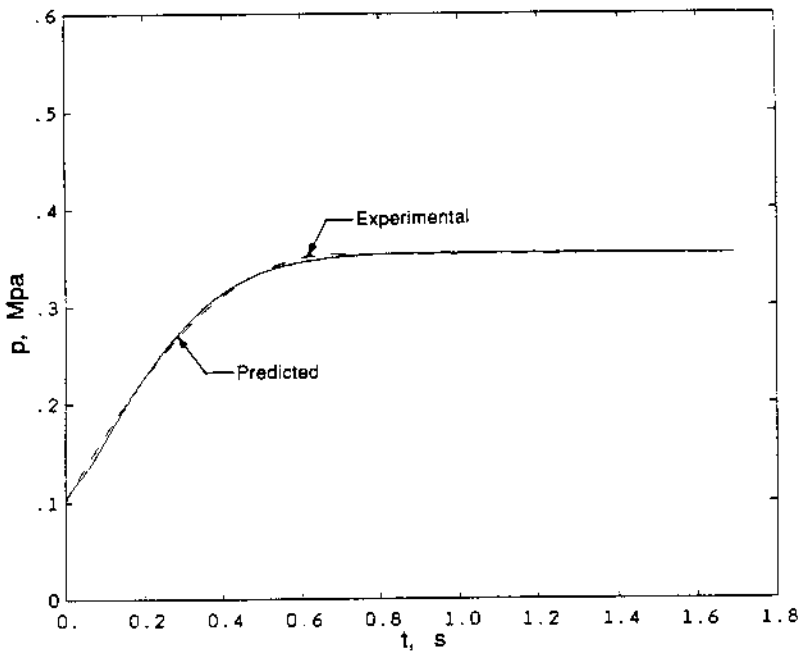

Figure 10a. Comparison between Predicted and Measured Pressure $p(t)$—Charging Process

would like to reduce such ripples to as small a variation as possible. Figure 6 indicates that the effect of ω_c on Δp is more significant than that of the other two parameters.

CONTROL STRATEGY

It has been shown that the proportional control alone is not sufficient because the steady-state error still exists. Thus, an integral control is added to the block diagram in Figure 7, where k_p is the proportional gain and k_i is the integral gain. To analyze the closed-loop system behavior, we assume that the carrier frequency ω_c is sufficiently large such that the effect of the carrier signal is small. Hence the transfer characteristics of the pulse width can be expressed as a pure gain. The open-loop transfer function is:

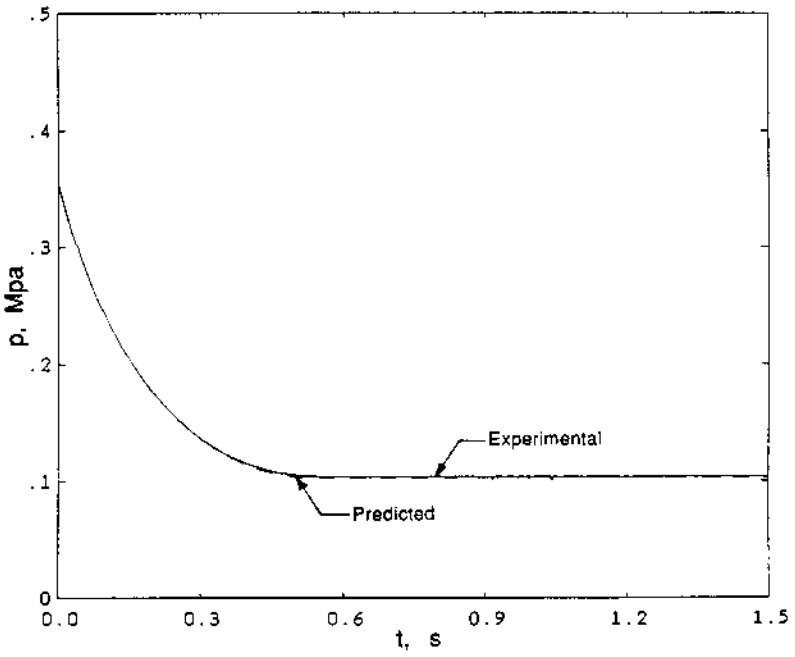

Figure 10b. Comparison between Predicted and Measured Pressure $p(t)$—Discharging Process

$$
\begin{aligned}
G(s) &= \frac{k_o(s+z)}{s(s+\tau)} \\
z &= \frac{k_i}{k_p} \\
k_o &= k_p k_a k_w \\
k_w &= \frac{A_{v1} + A_{v2}}{2h}
\end{aligned}
\tag{17}
$$

This is a Type 1 system, whose steady-state error is zero for a step input. Figure 8 illustrates the pole locations for the closed-loop system. It shows that as the zero z is moved to the left, the system bandwidth will increase, but, for same open-loop gain k_0, the system response may grow more oscillatory. This can be improved by either increasing k_p or decreasing h and hence increasing k_o, provided that it does not saturate the valve. However, since the coefficients B_{0m} and B_{1m} as shown in Equation 10 and Figure 2 can be reduced more significantly when h is decreased than when k_p is increased, we would like to take k_p = 1, and adjust the system gain by varying h.

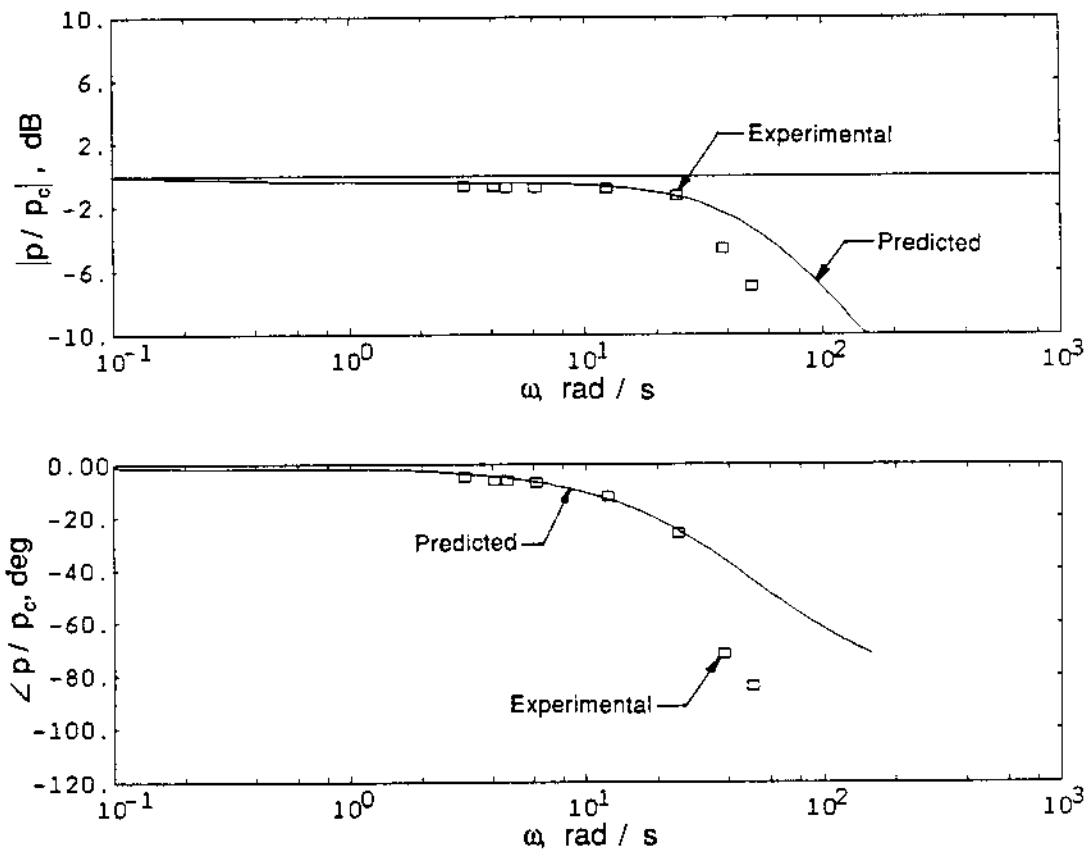

Figure 11. Comparison between Predicted and Measured Frequency Response

EXPERIMENTAL RESULTS

The experimental set-up (shown in Figure 9) consists of a pneumatic chamber with adjustable volume V, and a 3-way poppet valve (Parker No. T21025) operated by a solenoid, which is controlled by an electronic relay. A tank is connected to the supply port of the valve to regulate the supply pressure p_s. An Intel 86/310 microcomputer, with associated A/D (iSBX311) and D/A (iSBX328) converters of resolution 2.44 mv, is used as the controller. The pressure $p(t)$, measured with a strain gage type pressure transducer, is sent to a signal conditioner, and then to the A/D. The computer sends the output through D/A to the relay circuit to command the valve motion. The carrier signal $e_c(t)$ is generated digitally in the computer.

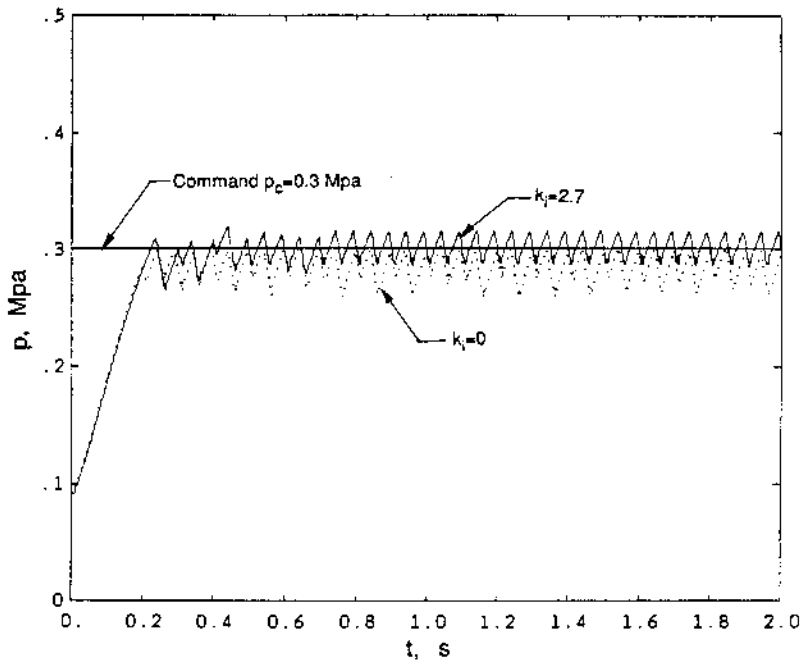

Figure 12. Effect of Integral Gain k_i on Measured Step Response

Predicted and measured pressure responses during the charging and discharging processes are compared in Figures 10a and 10b, respectively. We can see that the predictions using the nonlinear model given by Equations 3 and 4 agree with the measurements very well.

Figure 11 compares the predicted and measured frequency responses. For input frequencies that are below 4 Hz, the predictions match the measurements. But, if the input frequency is higher than 4 Hz, the measurements have smaller amplitudes and more phase lags than the predictions. This is due to the aliasing between the input $e_p(t)$ and the carrier signals $e_c(t)$ in the measurements. The effect of $e_c(t)$ is neglected in the model. Therefore, we can conclude that the input frequency ω cannot exceed a certain value, which is dictated by the aliasing problem, and the model given by Equations 3 and 4 can be used to represent the system only for a low frequency input.

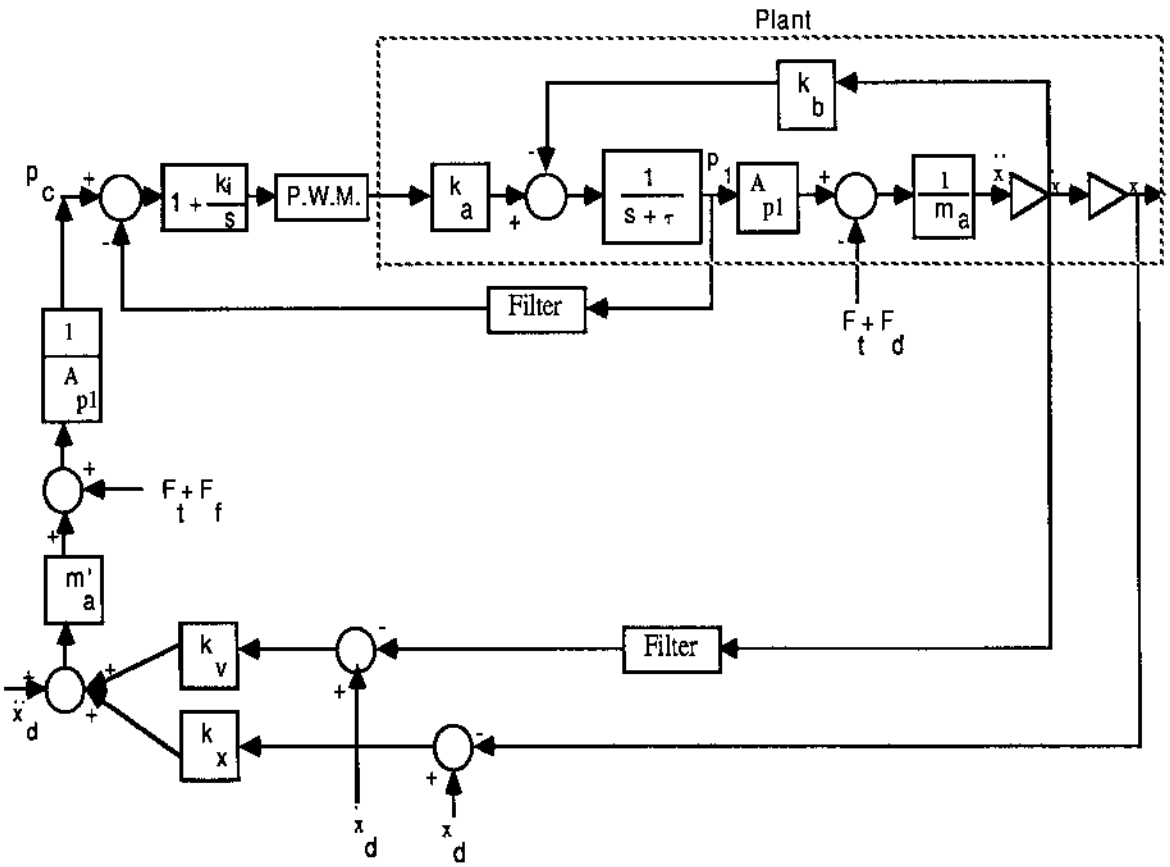

Figure 13. Displacement Control Strategy

Figure 12 illustrates that as an integral control is implemented, the steady-state error with the measured step response is reduced. In both cases, the sampling time T_s = 2 milliseconds and the pulse period T_p = 50 milliseconds. We would like T_p to be as small as possible, and, on the other hand, for T_s to be as large as possible. However, due to the limitation of the valve bandwidth, T_p cannot be too small. Also, to insure that there is a sufficient number of data inputs for each pulse cycle to the pulse-width modulator, T_s cannot be too large. Therefore, there is tradeoff between the selection of values for T_s and T_p.

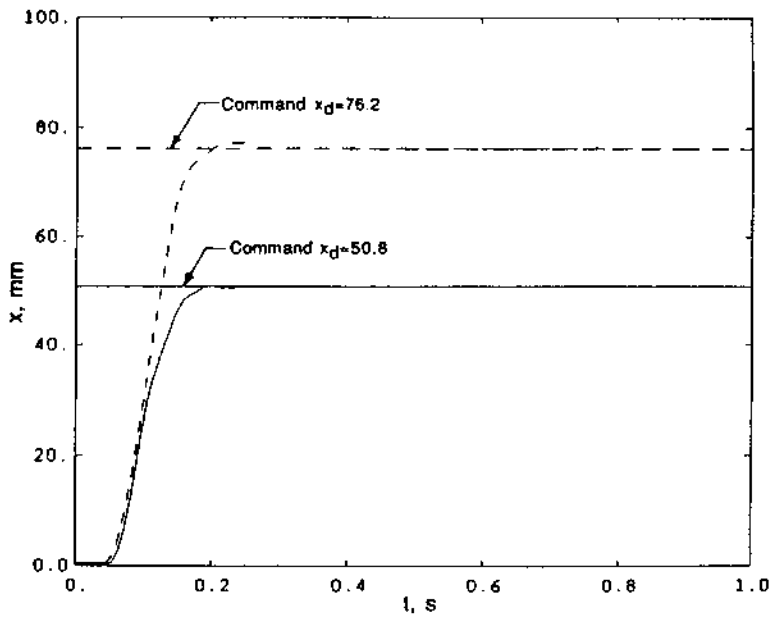

Figure 14. Measured Displacement Response

APPLICATION

The pressure control scheme has been applied to a pneumatic actuator for position control [Lai et al., Reference 5]. This pneumatic system is composed of two on-off valves in conjunction with a linear actuator carrying an external load. One valve is held open and the other valve is operated under PWM mode to simulate the proportional control. The block diagram of the system is shown in Figure 13. The outer-loop with displacement and velocity feedbacks is used to control the displacement, and the PI control scheme proposed in this paper is used in the inner-loop to control the pressure. This control system has been shown to be effective to achieve the desired actuation performance without using any mechanical stops in the actuator. One of the experimental results is shown in Figure 14. For more detail see Reference 5.

CONCLUSIONS

In this paper we have presented an analytical method to examine the effect of the PWM mode on the performance of a pneumatic valve-chamber system and have proposed a PI control strategy to control the pressure response. A flow direction dependent first-order chamber model incorporating the fundamental frequency component of the PWM mode has been used to study the system frequency response, and the governing differential equations have been solved to obtain the steady-state behavior. Our predictions agree with the measured data extremely well in the frequency domain and in the time domain as well during both charging and discharging processes. Simulation results also indicate that the increase in carrier frequency can enhance the system performance significantly. Experimental demonstration of the PI controller on a pneumatic chamber has been successful in achieving the desired pressure performance. This control strategy can be applied to pneumatic actuators or manipulators for position or force control.

REFERENCES

1. B.W. Andersen. *The Analysis and Design of Pneumatic Systems,* New York: John Wiley, 1967.
2. H.S. Black. *Modulation Theory,* New York: D. Van Nostrand, 1953.
3. L.R. Botting, G.T. Eynon and K. Foster. "The Response of a High-Pressure Pneumatic Servomechanism to Step and Sinewave Inputs," *Proc. Inst. Mech. Engrs.,* 1970, 184 (1), pp. 993-1012.
4. C.R. Burrows. "Effect of Position on the Stability of Pneumatic Servomechanism," *J. Mechanical Engineering Science,* 1969, 11 (6), pp. 615-616.
5. J.Y. Lai, C.H. Menq and R. Singh. "Accurate Position Control of a Pneumatic Actuator," submitted to the *J. Dynamic Systems, Measurement, and Control.*
6. S. Liu and J.E. Bobrow. "An Analysis of a Pneumatic Servo System and Its Application to a Computer-Controlled Robot," ASME Winter Annual Meeting, December 13-18, Boston MA, DSC-Vol. 6, pp. 385-392.
7. Y.S. Morita, M. Shimizu and T. Kagawa. "An Analysis on Pneumatic PWM and its Application to a Manipulator," *Proc. of International Symposium on Fluid Control and Measurement,* Tokyo, 1985, pp. 3-8.

8. T. Noritsugu. "Pulse-Width Modulated Feedback Force Control of a Pneumatically Powered Robot Hand," *Proc. of International Symposium on Fluid Control and Measurement*, Tokyo, 1985, pp. 47-52.
9. T. Noritsugu. "Development of PWM Mode Electro-Pneumatic Servomechanism, Part II: Position Control of a Pneumatic Cylinder," *J. Fluid Control*, Vol. 17, No. 1 (66), pp. 65-80.
10. S. Scavanda, A. Kellal and E. Richard. "Linearized Models for an Electropneumatic Cylinder Servovalve System," *Proc. of the 3rd International Conference in Advanced Robotics*, Oct. 13-15, 1987, France.
11. J.L. Shearer. "Study of Pneumatic Process in the Continuous Control of Motion with Compressed Air—I and II," *Trans. ASME*, pp. 233-242.
12. H.W. Shu, H.S. Cho and C. W. Lee. "Grasping Force Control for a Robot Gripper using Pneumatic On-Off Servomechanism," *Proc. of Control of Manufacturing Processes and Robotic Systems*, pp. 233-242.

NOMENCLATURE

A_{v1}	Valve orifice area, charging
A_{v2}	Valve orifice area, discharging
C_{d1}	Discharge coefficient with respect to input port
C_{d2}	Discharge coefficient with respect to output port
e_p	Error pressure
$e_p(t)$	Input signal to pulse-width modulator
E_0	Maximum amplitude of input sinusoidal wave
h	Amplitude of the carrier signal
k_i	Integral gain
k_p	Proportional gain
m	Mass
$\dot{m}$	Mass flow rate
n	Isentropic constant
$\bar{p}$	Operating pressure
Δp	Pressure ripple
$\bar{p}_a$	Average pressure
p_4	Atmospheric pressure
p_s	Supply pressure
$p(t)$	Chamber pressure
$p_c(t)$	Command chamber pressure
R	Gas constant
t	Time
T	Temperature
T_p	Pulse period

T_τ Duty pulse width
T_s Sampling time
$u(t)$ Periodic pulse signal
V Chamber volume
α Duty factor
τ Time constant
ω Modulating frequency
ω_c Carrier frequency